or CoW_{11}^{6-}, when 0.01 M LiCl was replaced by 0.01 M CsCl as the ionic-strength-controlling electrolyte, K_{exptl} was reduced to one-half (Table II) and k_q ($=k_d$) was reduced by about 30% (Table I).

While most of the experiments were carried out at $[RuL_3^{2+}]/[MW_{11}^{6-}]$ ratios much smaller than unity (vide supra), in some experiments an excess of RuL_3^{2+} was used. Figure 4 shows that under such conditions the I_0/I vs. [Q] Stern–Volmer plot for the $Ru(bpy)_3^{2+}$–MnW_{11}^{6-} system exhibits a quite peculiar shape, in contrast with the linear shape of the plot obtained when the MnW_{11}^{6-} quencher is in excess with respect to the $Ru(bpy)_3^{2+}$. In contrast, the τ_0/τ vs. [Q] plot is the same, regardless of the excess species. This shows that the different behavior of the I_0/I vs. [Q] plots has to be due to static quenching effects. The very peculiar behavior of the I_0/I vs. [Q] plot for $[Ru(bpy)_3^{2+}]/[MnPW_{11}^{6-}]$ ratios higher than unity is likely to be caused by the presence of variable amounts of 1:1 and 2:1 associated species. In the latter species, the same MnW_{11}^{6-} ion can quench statically two different $Ru(bpy)_3^{2+}$ excited states. The presence of such RuL_3^{2+}–MW_{11}^{6-}–RuL_3^{2+} ion triplets has been confirmed by high-intensity laser excitation experiments where the annihilation reaction of two RuL_3^{2+} excited states has been observed.[47]

The peculiar shape of the I_0/I vs. $[Ru(bpy)_3^{2+}]$ plot at constant (1.0×10^{-5} M) MnW_{11}^{6-} concentration (Figure 5) is also worth noticing. For an ideal system where only dynamic quenching takes place and the ionic strength is constant, I_0/I would be constant at any $Ru(bpy)_3^{2+}$ concentration and coincident with the τ_0/τ plot. Under the experimental conditions used (Figure 5) the ionic strength changed slightly (as shown by the slight changes in the τ_0/τ ratio). The observed large changes in the I_0/I ratio with increasing $[Ru(bpy)_3^{2+}]$ must thus be due again to static quenching effects. Clearly, there is an increase of the contribution of the static quenching with increasing $Ru(bpy)_3^{2+}$ concentration for $[Ru(bpy)_3^{2+}]/[MnW_{11}^{6-}]$ ratios lower than unity and then a decrease at higher $[Ru(bpy)_3^{2+}]$ concentrations. This behavior should reflect the different fractions of free $Ru(bpy)_3^{2+}$ and of 1:1 and 2:1 associated species. For $[Ru(bpy)_3^{2+}] \rightarrow \infty$, the I_0/I value should reflect the quenching of associated species with high $[Ru(bpy)_3^{2+}]/[MnW_{11}^{6-}]$ stoichiometric ratios on free $Ru(bpy)_3^{2+}$ excited states (i.e., it practically should tend to unity). For $[Ru(bpy)_3^{2+}] \rightarrow 0$, I_0/I should reach the value imposed by the static quenching in the 1:1 ion pair.

(47) In such experiments, which will be reported elsewhere, RuL_3^{2+} was $Ru(bpy)_2(biq)^{2+}$ or $Ru(bpy)_2(DMCH)^{2+}$.

Conclusions

By an appropriate choice of polypyridine–Ru(II) complex cations and heteropolytungstate anions we have been able to obtain systems in which the rate of electron-transfer quenching of the excited Ru complex can be tuned. Values of the ion-pair association constants have been obtained under various experimental conditions, and the effects of reactant concentration and ionic strength on the dynamic and static quenching processes have been investigated.

Taking advantage of the extensive formation of ion pairs, rate constants of intramolecular electron-transfer quenching processes have been directly measured or evaluated.

Acknowledgment. We thank Prof. A. von Zelewsky and Dr. P. Belser for samples of some of the Ru(II) complexes, Dr. M. Ciano for the electrochemical measurements, Prof. M. Maestri for the computer programs, and Dr. M. Taddia for atomic absorption analyses. We also thank G. Gubellini for technical assistance. Partial support from Ministero della Pubblica Istruzione is gratefully acknowledged.

Registry No. $Ru(bpy)_3Cl_2$, 14323-06-9; $Ru(bpy)_2(4,4'\text{-}Cl_2bpy)(PF_6)_2$, 75778-18-6; $Ru(bpy)_2(biq)(PF_6)_2$, 75777-91-2; $Ru(bpy)_2(DMCH)Cl_2$, 105817-79-6; $K_6Co(H_2O)SiW_{11}O_{39}$, 105785-76-0; $K_6Mn(OH)PW_{11}O_{39}$, 105834-58-0.

Supplementary Material Available: Tables reporting lifetime and intensity quenching data (3 pages). Ordering information is given on any current masthead page.

Contribution from the Chemistry Center, IVIC, Caracas 1020-A, Venezuela, Chemistry Department, Universidad Simón Bolivar, Caracas 1080-A, Venezuela, and Istituto Chimico "G. Ciamician", University of Bologna, Bologna 40126, Italy

Interaction of $(\mu\text{-H})_4Ru_4(CO)_{12}$ with Diphosphines in the Presence of Trimethylamine *N*-Oxide. X-ray Crystal Structure Analyses of $(\mu\text{-H})_4Ru_4(CO)_{10}(\mu\text{-}\{Ph_2P(CH_2)_nPPh_2\})$ (n = 1, 3, 4), $(\mu\text{-H})_4Ru_4(CO)_{10}(\mu\text{-}\{Ph_2PCH_2CH(CH_3)PPh_2\})$, and $(\mu\text{-H})_4Ru_4(CO)_{10}(\{Ph_2PCH_2CH(CH_3)PPh_2\})$

José Puga,*[1a] Alejandro Arce,[1b] Dario Braga,*[1c] Nicola Centritto,[1b] Fabrizia Grepioni,[1c] Rafael Castillo,[1a] and Julian Ascanio[1a]

Received June 2, 1986

The complexes $(\mu\text{-H})_4Ru_4(CO)_{10}(\mu\text{-}\{Ph_2P(CH_2)_nPPh_2\})$ (n = 1 (**1**), 3 (**3**), 4 (**4**)), $(\mu\text{-H})_4Ru_4(CO)_{10}(\mu\text{-}\{Ph_2PCH_2CH(CH_3)PPh_2\})$ (**2a**), $(\mu\text{-H})_4Ru_4(CO)_{10}\{Ph_2PCH_2CH(CH_3)PPh_2\}$ (**2b**), and $[(\mu\text{-H})_4Ru_4(CO)_{11}]_2\{Ph_2P(CH_2)_5PPh_2\}$ (**5a**) have been characterized by IR, ^1H NMR, and ^{31}P NMR spectroscopy. The structures of compounds **1**, **2a**, **2b**, **3**, and **4** have been determined by single-crystal X-ray diffractometry. The diphosphine ligands are seen to bridge a Ru–Ru bond of the tetrahedral Ru_4 cluster in **1**, **2a**, **3**, and **4**, while the diphosphine ligand adopts a chelating mode of bonding in **2b**. The hydride atoms in each of the structures were not located but were inferred from Ru–Ru bond lengths. They take up the same distribution of idealized C_s symmetry in all four structures. Where an asymmetric carbon atom is present (**2a** and **2b**) only one of the two possible diastereoisomeric forms is found in the solid. Crystal data: for **1**, a = 10.967 (5) Å, b = 19.720 (3) Å, c = 18.430 (3) Å, β = 104.56 (3)°, space group $P2_1/c$, Z = 4, final R = 0.055, R_w = 0.056; for **2a**, a = 17.79 (1) Å, b = 20.419 (6) Å, c = 11.395 (4) Å, β = 106.84 (5)°, space group Cc, Z = 4, final R = 0.038, R_w = 0.039; for **2b**, a = 11.219 (5) Å, b = 13.229 (2) Å, c = 15.226 (3) Å, α = 92.59 (2)°, β = 93.21 (2)°, γ = 100.99 (2)°, space group $P\bar{1}$, Z = 2, final R = 0.054, R_w = 0.059; for **3**, a = 8.783 (1) Å, b = 21.133 (6) Å, c = 22.140 (2) Å, β = 90.96 (1)°, space group $P2_1/c$, Z = 4, final R = 0.048, R_w = 0.049; for **4**, a = 8.918 (1) Å, b = 21.701 (3) Å, c = 22.131 (4) Å, β = 100.47 (1)°, space group Cc, Z = 4, final R = 0.034, R_w = 0.035.

Introduction

Tetranuclear carbonyl cluster have been shown to be useful catalysts, or catalyst precursors, for hydrogenation reactions.[2,3] Incorporation of bidentate phosphines within the metal framework configuration could be used, in some instances to maintain the

(1) (a) IVIC. (b) Universidad Simón Bolivar. (c) University of Bologna.

(2) Sánchez-Delgado, R. A.; Puga, J.; Rosales, M. *J. Mol. Catal.* **1984**, *24*, 221

0020-1669/87/1326-0867$01.50/0

Table I. Spectroscopic Data

compd[d]	$\delta(^1H)$[a]	J, Hz	$\delta(^{31}P)$[b]	J(P–P), Hz	IR[c] ν(CO), cm^{-1}
1	−16.90 (t)	3	10 (s)		2062 (s), 2043 (s), 2024 (vs), 2002 (s), 1972 (br), 1958 (br)
2a	−17.10 (t)	2	48.0 (d), 34.9 (d), 43.5 (d), 28.4 (d)	4.9 7.3	2068 (s), 2050 (vs), 2027 (vs), 2006 (s), 1990 (br), 1970 (br)
2b	−16.00 (br) −18.70 (br)		72.4 (d), 47.3 (d)	23	2066 (s), 2038 (vs), 2016 (vs), 2000 (s), 1990 (br), 1970 (br)
3	−17.16 (br)		28.5 (s)		2068 (s), 2048 (s), 2026 (vs), 2004 (s), 1989 (br), 1964 (br)
4	−17.30 (br)		28.2 (s)		2064 (s), 2046 (vs), 2024 (vs), 2006 (s), 1979 (br), 1955 (br)
5a	−15.40 (d)	2	28.6 (s)		2088 (m), 2080 (m), 2060 (s), 2050 (vs), 2020 (s), 2002 (br)
5b	−17.16 (br)		30.2 (s)		2070 (s), 2052 (vs), 2010 (vs), 2000 (sh), 1990 (br)

[a] In $CDCl_3$ at 100 MHz and 300 K. [b] In $CDCl_3$ at 24.298 MHz and 300 K, H_3PO_4 reference. [c] In cyclohexane solution. [d] Key: **1**, $(\mu\text{-H})_4Ru_4(CO)_{10}(\mu\text{-}\{Ph_2PCH_2PPh_2\})$; **2a**, $(\mu\text{-H})_4Ru_4(CO)_{10}(\mu\text{-}\{Ph_2PCH_2CH(CH_3)PPh_2\})$; **2b**, $(\mu\text{-H})_4Ru_4(CO)_{10}\{Ph_2PCH_2(CH_3)PPh_2\}$; **3**, $(\mu\text{-H})_4Ru_4(CO)_{10}(\mu\text{-}\{Ph_2P(CH_2)_3PPh_2\})$; **4**, $(\mu\text{-H})_4Ru_4(CO)_{10}(\mu\text{-}\{Ph_2P(CH_2)_4PPh_2\})$; **5a**, $[(\mu\text{-H})_4Ru_4(CO)_{11}]_2\{Ph_2(CH_2)_5PPh_2\}$.

nuclearity of the cluster, under the reaction conditions, bringing about an enhanced catalytic activity. The presence of asymmetric bidentate phosphine ligands within the cluster unit could, on the other hand, lead to potential catalysts for asymmetric hydrogenation. A chain-length effect on the preferred coordination mode of bidentate phosphines was suggested for trinuclear complexes.[4,5] The study of the binding of bidentate phosphines with $Ru_5C(CO)_{15}$ has shown that the coordination mode does depend on the chain length.[6,7] Isomerization processes involving change of the coordination mode of the diphosphine ligand have been observed during the reaction with pentanuclear and tetranuclear ruthenium clusters.[6,9] We have carried out a systematic study of the interaction of $(\mu\text{-H})_4Ru_4(CO)_{12}$ with $Ph_2(CH_2)_nPPh_2$ (n = 1, 3, 4, 5) and $Ph_2PCH_2CH(CH_3)PPh_2$, in the presence of trimethylamine *N*-oxide, in an attempt to investigate (a) the effect of the methylene chain length and the influence of introducing a methyl group into the chain on both coordination mode and the *bridged-chelate* isomerization process and (b) the conformational arrangements of the coordinated diphosphine ligands, the absolute configuration of the asymmetric carbon atom on coordination of $Ph_2PCH_2CH(CH_3)PPh_2$ in the solid state, and correlations between solid-state and solution-state behavior.

Results and Discussion

Treatment of $(\mu\text{-H})_4Ru_4(CO)_{12}$ with $Ph_2P(CH_2)_nPPh_2$ and $Ph_2PCH_2CH(CH_3)PPh_2$ (racemic mixture), in the presence of trimethylamine *N*-oxide, yields the substitution products $(\mu\text{-H})_4Ru_4(CO)_{10}(\mu\text{-}\{Ph_2P(CH_2)_nPPh_2\})$ (n = 1 (**1**), 3 (**3**), 4 (**4**)) and $(\mu\text{-H})_4Ru_4(CO)_{10}(\mu\text{-}\{Ph_2PCH_2CH(CH_3)PPh_2\})$ (**2a**) characterized by IR, ^1H NMR, and ^{31}P NMR spectroscopy (Table I). It is interesting to point out that these compounds showed an essentially identical IR pattern. This observation allowed us to establish the coordination mode of the diphosphine ligand in a very simple manner. The ^1H NMR spectra of these complexes showed that the signal observed at 300 K broadens as the temperature is decreased to 223 K. This result is in agreement with the information previously reported for $(\mu\text{-H})_4Ru_4(CO)_{10}(\mu\text{-}\{Ph_2P(CH_2)_2PPh_2\})$ (**2c**), which shows the fluxional character of the hydride ligands.[8,9]

^{31}P NMR Study of $(\mu\text{-H})_4Ru_4(CO)_{10}(\mu\text{-}\{Ph_2P(CH_2)_nPPh_2\})$ (n = 1 (1), 3 (3), 4 (4)), $(\mu\text{-H})_4Ru_4(CO)_{10}(\mu\text{-}\{Ph_2PCH(CH_3)CH_2PPh_2\})$ (2a), and $(\mu\text{-H})_4Ru_4(CO)_{10}\{Ph_2PCH(CH_3)CH_2PPh_2\}$ (2b). The ^{31}P NMR spectra of compounds **1**, **3**, and **4**, obtained at 300 K, showed only one signal attributed to the presence of two equivalent phosphorus nuclei (Table I). Taking into account the fluxional character of the hydride ligands at this temperature, these spectra could be explained in terms of (a) a symmetrical arrangement of the coordination mode of the diphosphine ligand or (b) rapid interconversion of conformers, on the NMR time scale, therefore achieving equivalence of the two phosphorus nuclei.

Scheme I

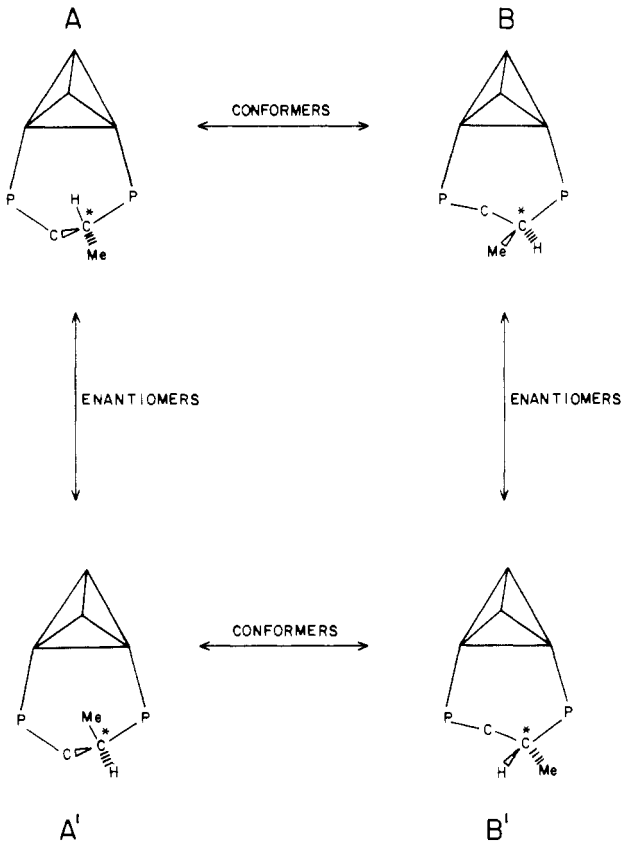

A symmetrical arrangement of the coordinated diphosphine could be expected in **1**. However that would not necessarily be the case as the length of the methylene chain is increased. In fact compound **2c** has been reported to possess two inequivalent phosphorus atoms both in the solid state and in solution.[9] We therefore carried out a variable-temperature ^{31}P NMR study and found that when compounds **1** (at 253 K in $CDCl_3$), **3**, and **4** (at 193 K, in toluene-d_8) were cooled, no change is observed. These facts seem to indicate that interconversion of conformers for compounds **3** and **4** is rapid, on the NMR time scale and occurs even at 193 K, showing the flexibility of the polymethylene chains in solution.

For **2a**, however, two pairs of doublets, of equal intensity, are observed in the ^{31}P NMR spectrum (Table I); this can be explained in terms of the presence of one or both pairs of conformers AB and A′B′ depicted in Scheme I. The ^{31}P NMR spectrum of **2a**

(3) (a) Doi, Y.; Koshizuka, K.; Keu, K. *Inorg. Chem.* **1982**, *21*, 2732. (b) Doi, Y.; Tamura, S.; Koshizuka, K. *J. Mol. Catal.* **1983**, *19*, 213.
(4) Cotton, F. A.; Hanson, B. A. *Inorg. Chem.* **1977**, *16* 3369.
(5) Bruce, M. I.; Shaw, G.; Stone, F. G. A. *J. Chem. Soc., Dalton Trans.* **1972**, 2094.
(6) Evans, J.; Gracey, B. P.; Gray, L. R.; Webster, M. *J. Organomet. Chem.* **1982**, *240*, C61.
(7) Johnson, B. F. G.; Lewis, J.; Nicholls, J. N.; Puga, J.; Raithby P. R.; Rosales, M. J.; McPartlin, M.; Clegg, W. *J. Chem. Soc., Dalton Trans.* **1983**, 277.
(8) Churchill, M. R.; Lashewycz, R. A. *Inorg. Chem.* **1978**, *17*, 1950.
(9) Churchill, M. R.; Lashewycz, R. A.; Shapley, J. R.; Richter, S. I. *Inorg. Chem.* **1980**, *19*, 1277.

obtained at 223 K, in $CDCl_3$, is essentially identical with that observed at 300 K; attempts to obtain the spectrum at 333 K led to formation of the chelate isomer **2b**. Reaction of $(\mu\text{-H})_4Ru_4(CO)_{12}$ with optically pure (*R*)-(+)-1,2-bis(diphenylphosphino)propane affords compound **2d**, which showed a ^{31}P NMR spectrum identical with that observed for **2a**. The spectrum obtained at 353 K in toluene-d_8 revealed formation of the chelate derivative.

The Bridge-Chelate Isomerization Process. The bridge-chelate isomerization process reported for **2c**[8,9] led us to investigate if compounds **1**, **2a**, **3**, and **4** undergo analogous conversion. Thus the complex $(\mu\text{-H})_4Ru_4(CO)_{10}(\mu\text{-}\{Ph_2PCH_2PPh_2\})$ (**1**) was refluxed in cyclohexane. The reaction was monitored by IR spectroscopy, and no change was observed after ca. 10 h. The fact that conversion into the chelate isomer does not take place, under the above conditions, could be attributed to the unfavorable energy requirements involved in the formation of a four-membered ring. The compound $(\mu\text{-H})_4Ru_4(CO)_{10}(\mu\text{-}\{Ph_2PCH_2CH(CH_3)PPh_2\})$ (**2a**) was also refluxed in cyclohexane, in an attempt to study the effect of the incorporation of a methyl group on the isomerization process. No change was observed in the IR spectrum of **2a** after 2h. This result is in contrast with that reported for $(\mu\text{-H})_4Ru_4(CO)_{10}(\mu\text{-}\{Ph_2P(CH_2)_2PPh_2\})$ (**2c**), which is extensively converted into the chelate isomer under the same conditions.[8,9] However formation of the chelate isomer $(\mu\text{-H})_4Ru_4(CO)_{10}\{Ph_2PCH_2CH(CH_3)\}$ (**2b**) does take place when **2a** is refluxed in cyclohexane for ca. 8 h, or better in $CHCl_3$ for 1.5 h. This result shows the effect of the methyl group incorporated. This conversion was monitored by ^{31}P NMR spectroscopy (Table I) and clearly indicates the solvent dependence of the bridged-chelate isomerization process. This observation suggests that an increase in solvent polarity enhanced phosphine dissociation to yield the chelate isomer, probably with formation of an intermediate possessing a diphosphine ligand coordinated in a monodentate fashion. No change was observed in the IR and ^{31}P NMR spectra of compounds **3** and **4** on dissolution in $CDCl_3$ at 60 °C for ca. 2 h or toluene-d_8 at 80 °C for ca. 2 h. This evidence clearly shows the dependence of the bridged-chelate isomerization process on the chain length.

Interaction of $(\mu\text{-H})_4Ru_4(CO)_{12}$ with $Ph_2P(CH_2)_5PPh_2$. Interaction of $(\mu\text{-H})_4Ru_4(CO)_{12}$ with $Ph_2P(CH_2)_5PPh_2$, in the presence of trimethylamine *N*-oxide, affords two different compounds characterized by IR, ^1H NMR, and ^{31}P NMR spectroscopy, Table I. The broad signal observed in the ^1H NMR spectrum of the red complex (**5a**), obtained at 233 K by using $CDCl_3$ as solvent, is resolved into a sharp doublet at 333 K. The variable-temperature ^{31}P NMR spectra of **5a** over the range 193–300 K, with toluene-d_8 used as solvent, showed one signal at 28.6 ppm. This evidence combined with the 20:8 integration ratio observed in the ^1H NMR spectrum for the phenyl groups and the hydride ligands, respectively, led us to formulate **5a** as $[(\mu\text{-H})_4Ru_4(CO)_{11}]_2\{Ph_2P(CH_2)_5PPh_2\}$. The ^1H NMR spectrum of the orange compound (**5b**), obtained at 333 K by using $CDCl_3$ as solvent, showed a triplet centered at −17.13 ppm, with $J = 7$ Hz. The signal broadens as the temperature is decreased. The variable-temperature ^{31}P NMR spectra over the range 193–300 K, with toluene-d_8 used as solvent, showed one signal at 30.2 ppm. Although the nature of compound **5b** is uncertain, the infrared pattern exhibited by this complex is totally different from that observed for the species $(\mu\text{-H})_4Ru_4(CO)_{10}(\mu\text{-}\{Ph_2P(CH_2)_nPPh_2\})$ herein reported. Furthermore compound **5b** presents an IR pattern more akin to $[(\mu\text{-H})_4Ru_4(CO)_{11}]_2\{Ph_2P(CH_2)_5PPh_2\}$ (**5a**).

Description of the Structure. The molecular structures of **1**, **2a**, **2b**, **3**, and **4** have been determined by single-crystal X-ray diffractometry. All these species are based on a tetrahedral core of Ru atoms with the non-hydrogen ligands retaining the conformation of the CO groups in the parent $H_4Ru_4(CO)_{12}$.[10] The bidentate phosphine ligand is found bridging a Ru–Ru bond in **1**, **2a**, **3**, and **4**, while it adopts a chelating bonding mode in **2b**. The four hydrogen ligands are inferred to be in the same geometry

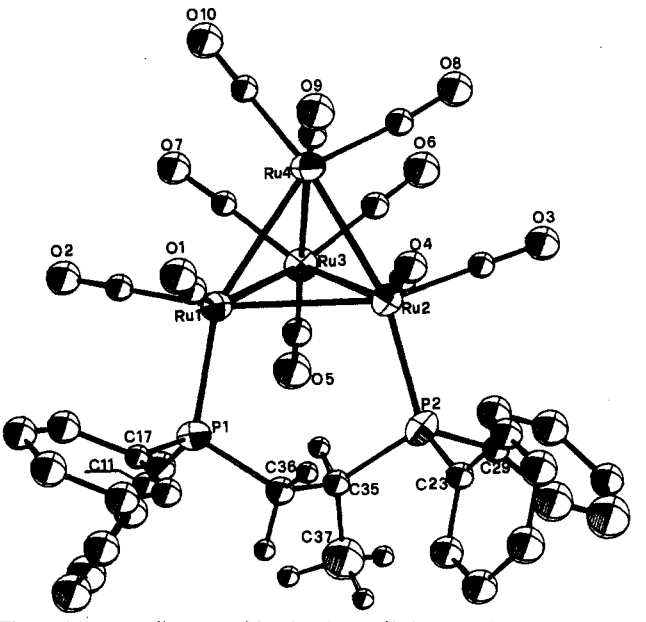

Figure 1. ORTEP diagram of **2a** showing 50% thermal ellipsoids. The C atoms of the CO groups bear the same numbering as the corresponding O atoms. Phenyl H atoms and C labels are omitted for clarity.

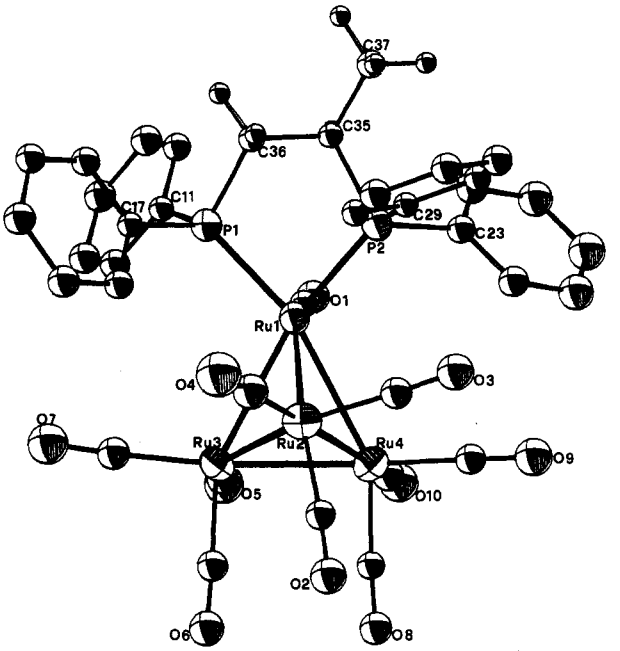

Figure 2. ORTEP diagram of **2b**, showing 50% thermal ellipsoids. The C atoms of the CO groups bear the same numbering as the corresponding O atoms. Phenyl H atoms and C labels are omitted for clarity.

in all four molecules, bridging four tetrahedron edges, three of which are around a triangular face (vide infra). Because of the close relationship existing among these species, they will be discussed together. In order to facilitate the comparison of the structural parameters, a common labeling scheme has been chosen by adopting the H-bridged Ru–Ru bonds as reference. Considering the three consecutive H-bridged Ru–Ru bonds as constituting a basal plane of the tetrahedral cluster, the positions of the substituent P atoms may be defined as axial or radial according to their orthogonal or coplanar location with respect to this plane, so that **1**, **2a**, **3**, and **4** show a bis-axial substitution, while **2b** shows an axial–radial disubstitution on the same Ru atom.

The molecular geometries of **2a** and **2b** are shown in Figure 1 and 2, respectively, while simplified structural models for all species herein discussed are grouped in Figure 3. The most relevant structural parameters for **1**, **2a**, **2b**, **3**, and **4** are reported in Table II.

(10) Wilson, R. D.; Wu, S. M.; Love, R. A.; Bau, R. *Inorg. Chem.* **1978**, *17*, 1221.

Table II. Relevant Bond Distances (Å) and Angles (deg)

	1		2a		2b		3		4
"Long"									
Ru(1)–Ru(2)	2.977 (2)		3.000 (2)		3.011 (1)		3.061 (1)		3.004 (2)
Ru(1)–Ru(3)	2.974 (2)		2.961 (2)		3.001 (1)		2.993 (1)		2.964 (1)
Ru(1)–Ru(4)	2.950 (2)		2.973 (2)		2.975 (1)		2.984 (2)		2.983 (2)
Ru(2)–Ru(3)	2.908 (2)		2.944 (2)		2.927 (1)		2.925 (2)		2.952 (2)
mean	2.952 (2)		2.970 (2)		2.979 (1)		2.991 (2)		2.976 (2)
"Short"									
Ru(2)–Ru(4)	2.756 (2)		2.759 (2)		2.772 (1)		2.769 (2)		2.782 (2)
Ru(3)–Ru(4)	2.775 (2)		2.770 (2)		2.784 (1)		2.790 (1)		2.795 (2)
mean	2.766 (2)		2.765 (2)		2.778 (1)		2.780 (2)		2.789 (2)
Ru(1)–P(1)	2.361 (6)		2.335 (5)		2.318 (3)		2.355 (3)		2.334 (3)
Ru(2)–P(2)	2.331 (6)		2.351 (5)		2.303 (3)		2.353 (4)		2.364 (4)
mean	2.346 (6)		2.343 (5)		2.311 (3)		2.354 (4)		2.349 (4)
P(1)–C(35)	1.83 (2)	P(1)–C(36)	1.82 (2)	P(1)–C(36)	1.81 (1)	P(1)–C(35)	1.85 (1)	P(1)–C(38)	1.79 (1)
P(2)–C(35)	1.85 (2)	P(2)–C(35)	1.87 (2)	P(2)–C(35)	1.86 (1)	P(2)–C(37)	1.87 (1)	P(2)–C(35)	1.85 (1)
		C(35)–C(36)	1.50 (2)	C(35)–C(36)	1.56 (2)	C(35)–C(36)	1.55 (2)	C(35)–C(36)	1.53 (2)
		C(35)–C(37)	1.48 (2)	C(35)–C(37)	1.55 (2)	C(36)–C(37)	1.51 (2)	C(36)–C(37)	1.54 (2)
								C(37)–C(38)	1.53 (2)
				Average Values					
Ru–C	1.86 (4)		1.85 (2)		1.84 (3)		1.86 (3)		1.84 (3)
C–O	1.17 (2)		1.15 (2)		1.17 (1)		1.16 (3)		1.17 (3)
P–C(Ph)	1.81 (1)		1.82 (1)		1.81 (1)		1.83 (1)		1.82 (1)
Ru–C–O	176 (2)		177 (2)		177 (1)		176 (2)		176 (1)
Ru–P–C	115 (1)		115 (1)		114 (1)		116 (1)		115 (1)
P–C–P	117 (1)								
P–C–C			116 (1)		111 (1)		112 (1)		115 (1)
C–C–C			107 (2)		110 (1)		116 (1)		114 (1)

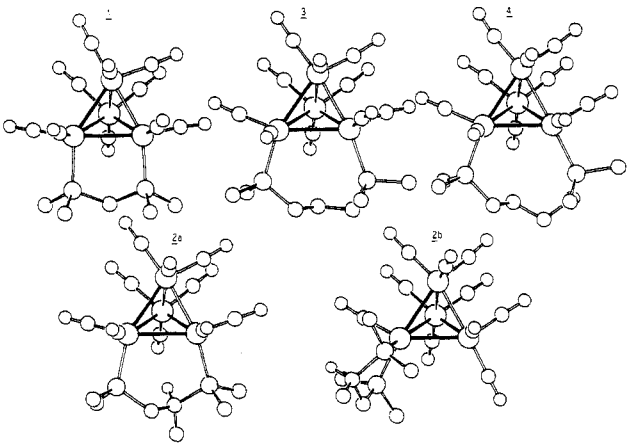

Figure 3. Structural models for **1**, **2a**, **2b**, **3**, and **4**. Solid bonds are bridged by the H atoms. Phenyl rings are omitted for clarity.

The four Ru atoms define a distorted tetrahedron with four "long" (solid bonds in Figure 3) and two "short" Ru–Ru bonds. The four "long" bonds are expected to bear the bridging hydrides as can be easily inferred on the basis of both metal–metal bond lengthening and CO ligand displacement. Direct location of the H(hydride) atoms from X-ray data of the kind illustrated by Churchill and co-workers[8,9] was not satisfactorily achieved in any of our cases (see Experimental Section). No substantial differences are shown in the average lengths for the two sets of Ru–Ru bonds (see Table II). Good agreement can also be seen with the values reported for other bidentate phosphine substituted derivatives such as $H_4Ru_4(CO)_{10}Ph_2P(CH_2)_2PPh_2$ [2.970 (1), 2.791 (1) Å][8] and $H_4Ru_4(CO)_{10}(\mu\text{-}Ph_2P(CH_2)_2PPh_2)$ [2.989 (2), 2.781 (2) Å],[9] with the values reported for disubstituted species such as $H_4Ru_4(CO)_{10}(PPh_3)_2$ [2.966 (1) Å], and finally with the values reported for the parent $H_4Ru_4(CO)_{12}$ species [2.950 (1), 2.786 (1) Å].[10] Interestingly the longest Ru–Ru bond is always Ru(1)–Ru(2), i.e. the one bridged by the bidentate phosphine in **1**, **2a**, **3**, and **4**, while the shortest among the H-bridged bonds [Ru(2)–Ru(3)] is systematically found opposite to the fourth 'out-of-base' H-bridged bond [Ru(1)–Ru(4)].

Chart I

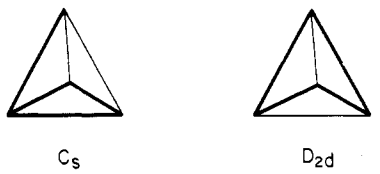

It is noteworthy that although ^1H NMR data indicate high fluxionality of the H(hydride) atoms even at low temperature, only one ordered distribution of these atoms has been observed in the solid-state structures of the diphosphine substituted species. Chart I shows the two possible arrangements of edge-bridging hydrides around a tetrahedral cluster. The more symmetric D_{2d} arrangement has been reported for the precursor $H_4Ru_4(CO)_{12}$ and for $H_4Ru_4(CO)_{10}PPh_3)_2$,[10] while a C_s arrangement has been found not only in all the species here discussed but also for both the aforementioned bridged and chelate $PPh_2(CH_2)_2PPh_2$-substituted species.[8,9]

The variation in the distribution of bridging hydrogen atoms may depend on a delicate balance of steric and electronic effects. In the present derivatives, nonbonding interactions may be alleviated by placing a bridging H atom on the same edge bridged by the bidentate phosphine ligands. Additionally, in the C_s structure, the H atoms attain maximum proximity to the electron-rich Ru atoms, i.e. those which bear the aliphatic phosphine ligands. The C_s structure contains five Ru(P-bonded)–H(bridging) interactions, Ru(1) being involved in three of these and Ru(2) in two. By contrast, the D_{2d} arrangement of bridging H atoms in $H_4Ru_4(CO)_{10}(PPh_3)_2$ may be attributed to differing steric and electronic effects. These ligands are in the first place less basic than the alkyl phosphines. In addition, when placed on opposite sides of the unbridged Ru–Ru bond,[10] these bulky ligands push adjacent CO groups into closer contact, which may be alleviated by the observed placement of the bridging hydrogen atoms.

The effect of lengthening the aliphatic chain belonging to the bridging diphosphine ligands is well reflected by the increase of the P–Ru–Ru angles in the P(1)–Ru(1)–Ru(2)–P(2) plane; mean values are 92.0 (1)° in **1**, 102.5 (1)° in **2a**, 107.7 (1)° in **3**, and 113.3 (1)° in **4**. The Ru_r–P–C_r (r = ring atoms) angles follow

Table III. Crystal Data and Intensity Collection Parameters

	1	2a	2b	3	4
formula	$C_{35}H_{26}O_{10}P_2Ru_4$	$C_{37}H_{30}O_{10}P_2Ru_4$	$C_{37}H_{30}O_{10}P_2Ru_4 \cdot 0.47(CH_2Cl_2)$	$C_{37}H_{30}O_{10}P_2Ru_4$	$C_{38}H_{32}O_{10}P_2Ru_4$
fw	1072.81	1100.86	1143.21	1100.86	1114.89
cryst syst	monoclinic	monoclinic	triclinic	monoclinic	monoclinic
a, Å	10.967 (5)	17.79 (1)	11.219 (5)	8.783 (1)	8.918 (1)
b, Å	19.720 (3)	20.419 (6)	13.229 (2)	21.133 (6)	21.701 (3)
c, Å	18.430 (3)	11.395 (4)	15.226 (3)	22.140 (2)	22.131 (4)
α, deg	90	90	92.59 (2)	90	90
β, deg	104.56 (3)	106.84 (5)	93.21 (2)	90.96 (1)	100.47 (1)
γ, deg	90	90	100.99 (2)	90	90
V, Å^3	3857.0	3962.4	2211.2	4109.1	4211.7
d(calcd), g/cm^3	1.84	1.84	1.72	1.84	1.83
Z	4	4	2	4	4
space group	$P2_1/c$	Cc	$P\bar{1}$	$P2_1/c$	Cc
F(000)	2088	2152	1096	2152	2184
cryst color	orange	orange	dark yellow	dark yellow	dark yellow
cryst size, mm	0.2 × 0.2 × 0.5	0.25 × 0.2 × 0.1	0.1 × 0.2 × 0.1	0.5 × 0.2 × 0.2	0.7 × 0.7 × 0.1
μ(Mo Kα), cm^{-1}	15.1	14.7	13.8	14.2	13.8
θ range, deg	2.5–25	2.5–25	2.5–23	2.5–25	2.5–25
scan type[a]	$\omega/2\theta$	$\omega/2\theta$	$\omega/2\theta$	$\omega/2\theta$	$\omega/2\theta$
scan interval,[d] deg	0.8	1.3	1.3	0.7	0.7
prescan, speed, deg/min	5	8	5	5	6
prescan $\sigma(I)/I$	0.5	0.5	0.5	0.5	0.5
required final $\sigma(I)/I$	0.02	0.01	0.02	0.02	0.02
max time, sec	150	150	140	150	150
octants collecd	$\pm h,+k,+l$	$\pm h,+k,+l$	$\pm h,\pm k,+l$	$\pm h,+k,+l$	$\pm h,+k,+l$
no. of indep data	5289	3325	5361	5866	3923
no. of data with $I > 2.5\sigma(I)$	2336	2324	3793	3177	2199
equiv reflcns merging	0.1	0.02	0.03	0.05	0.0
abs corr type[b]	ψ scan (250)	WS	WS	WS	ψ scan (330)
corr range, %	66–100	90–100	90–100	93–100	97–99
R, R_w[c]	0.055; 0.056	0.038; 0.039	0.054; 0.059	0.048; 0.049	0.034; 0.035
K; g[c]	1.74; 0.0013	1.58; 0.0005	1.93; 0.001	2.51; 0.0004	1.20; 0.0005

[a] Background time = peak scanning time for all measurements. [b] Scan and WS indicate whether the correction was applied by measuring azimutal reflections, or by using the Walker and Stuart method (see Experimental Section). [c] $R_w = \sum[(F_o - F_c)w^{1/2}]/\sum(F_o w^{1/2})$, where $w = K/[\sigma^2(F) + |g|F^2]$; the values for k, and g are reported. [d] +0.35 tan θ.

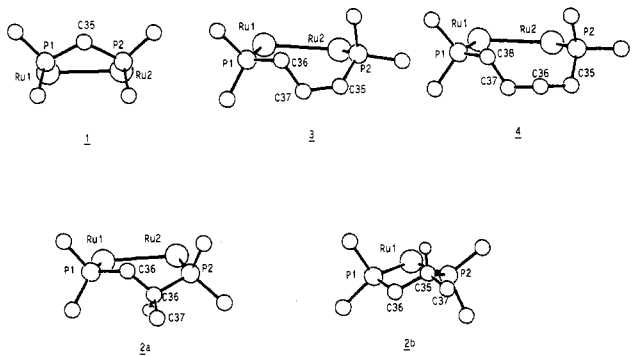

Figure 4. Comparison of the Ru–P–C_n–P–Ru ring conformation for **1**, **2a**, **2b**, **3**, and **4**.

the same trend: in fact, while a reasonable tetrahedral angle of 109.5 (1)° is found in **1**; this value increases up to 119.0 (1)° in **4**, indicating that further lengthening of the aliphatic chain leads to more tense steric situations and is certainly unfavored. This consideration is somewhat strengthened by looking at the structure of the pentanuclear complex $Ru_5C(CO)_{15}(\mu\text{-}Ph_2P(CH_2)_4PPh_2)$[6] where the bidentate ligand bridges two *opposite* rather than two consecutive Ru atoms of the Ru_5 square base, thus decreasing the strains within the eight-membered ring. These facts may account for the formation of dimers via CO monosubstitution with longer chains as discussed above.

A comparison of Ru–P–C_n–P–Ru (n = 1, 4) ring conformations indicates that the P–Ru–Ru–P system in **1**, **2a**, **3**, and **4** is almost planar (maximum elevation from the plane of 0.12 Å observed in **3**) while the carbon chains give "twisted" conformations, which can be assimilated to those shown by cycloalkenes (see Figure 4). A further point of interest is the fact that the aliphatic chains, because of the presence of the bulky phenyl groups on the P atoms, are forced to pucker always *under* the cluster basal plane.

Scheme II

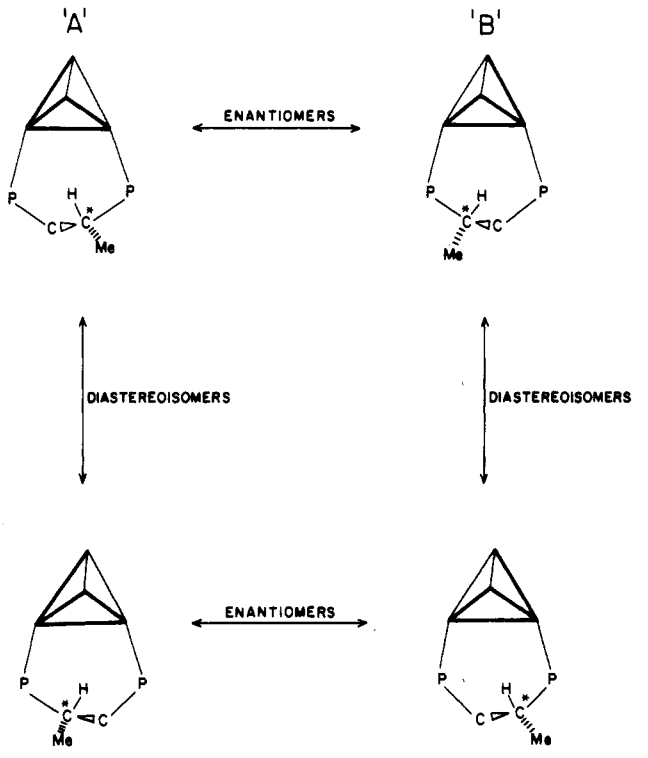

A different situation is obviously observed in **2b**, where the bidentate phosphine ligand chelates Ru(1) by radial–axial substitution of two COs. The five-membered ring so generated presents a P(1)–Ru(1)–P(2) angle of 84.0 (1)°, which although it may seem very acute [average C–Ru–C = 94 (2)°], does not

Table IV. Fractional Atomic Coordinates and Thermal Parameters (Å^2) for **1**

atom	x	y	z	U_{iso} or U_{eq}
Ru(1)	0.00455 (16)	0.03285 (8)	0.23253 (9)	0.0325 (10)
Ru(2)	0.00743 (16)	0.18269 (8)	0.25262 (9)	0.0374 (10)
Ru(3)	0.00131 (15)	0.12670 (8)	0.10575 (8)	0.0342 (10)
Ru(4)	0.21632 (15)	0.12193 (9)	0.22338 (9)	0.0393 (11)
P(1)	−0.2062 (5)	0.0258 (3)	0.2412 (3)	0.035 (3)
P(2)	−0.1984 (5)	0.1838 (3)	0.2660 (3)	0.041 (3)
C(1)	0.0843 (21)	−0.0065 (11)	0.3243 (13)	0.050 (6)
O(1)	0.1386 (17)	−0.0274 (9)	0.3819 (10)	0.076 (5)
C(2)	0.0003 (23)	−0.0507 (12)	0.1801 (13)	0.060 (7)
O(2)	−0.0029 (17)	−0.0988 (10)	0.1450 (10)	0.085 (5)
C(3)	0.0175 (23)	0.2699 (13)	0.2277 (13)	0.061 (7)
O(3)	0.0100 (18)	0.3272 (11)	0.2064 (11)	0.096 (6)
C(4)	0.1033 (23)	0.2047 (11)	0.3485 (13)	0.057 (7)
O(4)	0.1695 (21)	0.2134 (11)	0.4083 (13)	0.108 (7)
C(5)	−0.1475 (24)	0.1315 (13)	0.0287 (14)	0.067 (7)
O(5)	−0.2335 (19)	0.1349 (10)	−0.0243 (11)	0.097 (6)
C(6)	0.0749 (24)	0.1980 (13)	0.0736 (14)	0.065 (7)
O(6)	0.1243 (19)	0.2468 (10)	0.0542 (11)	0.093 (6)
C(7)	0.0894 (24)	0.0655 (13)	0.0560 (14)	0.066 (7)
O(7)	0.1410 (16)	0.0273 (9)	0.0287 (9)	0.077 (5)
C(8)	0.2670 (26)	0.2116 (14)	0.2202 (15)	0.076 (8)
O(8)	0.2998 (20)	0.2678 (11)	0.2148 (11)	0.100 (6)
C(9)	0.3128 (25)	0.1087 (13)	0.3186 (15)	0.072 (7)
O(9)	0.3803 (19)	0.0994 (10)	0.3797 (11)	0.099 (6)
C(10)	0.3331 (22)	0.0849 (11)	0.1733 (12)	0.052 (6)
O(10)	0.4082 (18)	0.0623 (10)	0.1491 (10)	0.088 (6)
C(12)	−0.3283 (13)	0.0292 (6)	0.3582 (7)	0.053 (6)
C(13)	−0.3512 (13)	0.0059 (6)	0.4251 (7)	0.065 (7)
C(14)	−0.2832 (13)	−0.0490 (6)	0.4625 (7)	0.057 (6)
C(15)	−0.1921 (13)	−0.0805 (6)	0.4332 (7)	0.068 (7)
C(16)	−0.1692 (13)	−0.0572 (6)	0.3664 (7)	0.055 (6)
C(11)	−0.2373 (13)	−0.0023 (6)	0.3289 (7)	0.047 (6)
C(18)	−0.3075 (14)	−0.0190 (7)	0.0980 (8)	0.064 (7)
C(19)	−0.3818 (14)	−0.0607 (7)	0.0432 (8)	0.090 (9)
C(20)	−0.4549 (14)	−0.1117 (7)	0.0636 (8)	0.085 (8)
C(21)	−0.4536 (14)	−0.1210 (7)	0.1388 (8)	0.098 (9)
C(22)	−0.3793 (14)	−0.0793 (7)	0.1937 (8)	0.068 (7)
C(17)	−0.3063 (14)	−0.0283 (7)	0.1733 (8)	0.037 (5)
C(24)	−0.3397 (11)	0.2047 (7)	0.3722 (7)	0.057 (6)
C(25)	−0.3582 (11)	0.2021 (7)	0.4443 (7)	0.067 (7)
C(26)	−0.2633 (11)	0.1772 (7)	0.5036 (7)	0.072 (7)
C(27)	−0.1497 (11)	0.1550 (7)	0.4908 (7)	0.073 (7)
C(28)	−0.1312 (11)	0.1576 (7)	0.4187 (7)	0.047 (6)
C(23)	−0.2261 (11)	0.1824 (7)	0.3594 (7)	0.045 (5)
C(30)	−0.4022 (15)	0.2461 (7)	0.1609 (9)	0.055 (6)
C(31)	−0.4733 (15)	0.3028 (7)	0.1309 (9)	0.084 (9)
C(32)	−0.4407 (15)	0.3667 (7)	0.1622 (9)	0.081 (8)
C(33)	−0.3370 (15)	0.3739 (7)	0.2236 (9)	0.103 (10)
C(34)	−0.2660 (15)	0.3172 (7)	0.2537 (9)	0.071 (7)
C(29)	−0.2986 (15)	0.2533 (7)	0.2223 (9)	0.056 (6)
C(35)	−0.2833 (19)	0.1084 (10)	0.2190 (11)	0.043 (5)

lead to an abnormally close P··P contact. The P(1)··P(2) contact [3.10 (1) Å] is in fact strictly comparable with that observed for the five-membered ring in **1** [3.14 (1) Å]. Moreover both Ru_r–P–C_r and P–C_r–C_r (r = ring atoms) show values that conform to tetrahedral P and C atoms [109 (1)° and 109 (1)°, respectively]. These fact may be taken as indicative that the five-membered ring in **2b** allows an ideal geometry. Therefore one of the reasons why the bridge-chelate isomerization does not occur for **1** is that a four-membered ring would be far too stressed. On the other hand longer aliphatic chains (i.e. larger rings) would require unfavored deformations of the "$RuP_2(CO)$" system. Bridge-chelate interconversion of a six-membered into a five-membered ring has been also reported for the intramolecular reaction of the tetrasubstituted $Ir_4(CO)_8\{\mu\text{-}Ph_2P(CH)_2PPh_2\}_2$ to give the ortho-metalated species $HIr_4(CO)_7\{\mu\text{-}Ph_2P(CH)_2PPh_2\}\{\mu_3\text{-}Ph_2P(CH)_2PPh(C_6H_4)\}$.[11] Decrease of the steric tensions within the former species upon conversion into the latter was invoked to account for the observed chemical behavior.

(11) Albano, V. G.; Braga, D.; Ros, R.; Scrivanti, A. *J. Chem. Soc., Chem. Commun.* **1985**, 866.

Table V. Fractional Atomic Coordinates and Thermal Parameters (Å^2) for **2a**

atom	x	y	z	U_{iso} or U_{eq}
Ru(1)	0.62327 (10)	0.34061 (5)	0.62866 (15)	0.0356 (7)
Ru(2)	0.59768 (10)	0.20366 (6)	0.70431 (15)	0.0332 (7)
Ru(3)	0.73694 (10)	0.27828 (6)	0.84198 (16)	0.0345 (7)
Ru(4)	0.58800	0.30473 (6)	0.86000	0.0364 (7)
P(1)	0.6505 (3)	0.3235 (2)	0.4425 (4)	0.043 (2)
P(2)	0.6375 (3)	0.1392 (2)	0.5620 (4)	0.040 (2)
C(1)	0.5216 (11)	0.3688 (9)	0.5477 (17)	0.057 (5)
O(1)	0.4601 (10)	0.3862 (7)	0.5054 (14)	0.091 (4)
C(2)	0.6715 (10)	0.4235 (8)	0.6507 (15)	0.049 (4)
O(2)	0.7076 (9)	0.4705 (7)	0.6694 (13)	0.080 (4)
C(3)	0.5990 (10)	0.1355 (8)	0.8098 (15)	0.046 (4)
O(3)	0.5973 (9)	0.0913 (7)	0.8473 (14)	0.081 (4)
C(4)	0.4914 (10)	0.2000 (8)	0.6472 (15)	0.046 (4)
O(4)	0.4243 (9)	0.1995 (6)	0.6092 (13)	0.073 (4)
C(5)	0.8362 (12)	0.2592 (9)	0.8263 (17)	0.057 (5)
O(5)	0.9001 (10)	0.2507 (8)	0.8237 (14)	0.095 (5)
C(6)	0.7521 (11)	0.2328 (8)	0.9870 (17)	0.051 (4)
O(6)	0.7636 (9)	0.2045 (7)	1.0772 (15)	0.088 (4)
C(7)	0.7654 (10)	0.3571 (8)	0.9226 (14)	0.044 (4)
O(7)	0.7854 (8)	0.4073 (7)	0.9690 (12)	0.074 (4)
C(8)	0.5852 (11)	0.2423 (8)	0.9750 (16)	0.051 (4)
O(8)	0.5834 (9)	0.2058 (7)	1.0534 (14)	0.083 (4)
C(9)	0.4802 (11)	0.3139 (8)	0.8130 (16)	0.052 (4)
O(9)	0.4137 (10)	0.3202 (8)	0.7886 (15)	0.094 (5)
C(10)	0.6101 (10)	0.3773 (8)	0.9669 (16)	0.050 (4)
O(10)	0.6212 (9)	0.4223 (7)	1.0297 (15)	0.087 (4)
C(12)	0.7517 (8)	0.3649 (7)	0.3138 (9)	0.086 (7)
C(13)	0.8256 (8)	0.3746 (7)	0.2973 (9)	0.106 (8)
C(14)	0.8931 (8)	0.3651 (7)	0.3951 (9)	0.103 (8)
C(15)	0.8867 (8)	0.3459 (7)	0.5093 (9)	0.077 (6)
C(16)	0.8128 (8)	0.3362 (7)	0.5257 (9)	0.062 (5)
C(11)	0.7453 (8)	0.3457 (7)	0.4280 (9)	0.046 (4)
C(18)	0.5829 (7)	0.4347 (5)	0.3249 (10)	0.072 (6)
C(19)	0.5264 (7)	0.4716 (5)	0.2403 (10)	0.076 (6)
C(20)	0.4688 (7)	0.4402 (5)	0.1476 (10)	0.088 (7)
C(21)	0.4678 (7)	0.3720 (5)	0.1396 (10)	0.079 (6)
C(22)	0.5243 (7)	0.3352 (5)	0.2243 (10)	0.059 (5)
C(17)	0.5818 (7)	0.3666 (5)	0.3170 (10)	0.039 (4)
C(24)	0.5720 (7)	0.0879 (6)	0.3245 (11)	0.072 (6)
C(25)	0.5146 (7)	0.0539 (6)	0.2359 (11)	0.084 (6)
C(26)	0.4485 (7)	0.0298 (6)	0.2638 (11)	0.097 (8)
C(27)	0.4398 (7)	0.0396 (6)	0.3803 (11)	0.091 (7)
C(28)	0.4972 (7)	0.0736 (6)	0.4689 (11)	0.071 (6)
C(23)	0.5633 (7)	0.0978 (6)	0.4409 (11)	0.051 (4)
C(30)	0.7613 (8)	0.0792 (5)	0.7378 (11)	0.078 (6)
C(31)	0.8108 (8)	0.0273 (5)	0.7895 (11)	0.090 (7)
C(32)	0.8011 (8)	−0.0335 (5)	0.7311 (11)	0.076 (6)
C(33)	0.7420 (8)	−0.0423 (5)	0.6211 (11)	0.131 (11)
C(34)	0.6926 (8)	0.0096 (5)	0.5694 (11)	0.110 (9)
C(29)	0.7023 (8)	0.0704 (5)	0.6278 (11)	0.046 (4)
C(35)	0.6947 (10)	0.1920 (8)	0.4851 (15)	0.047 (4)
C(36)	0.6417 (11)	0.2380 (8)	0.3950 (16)	0.055 (5)
C(37)	0.7494 (18)	0.1640 (14)	0.4230 (28)	0.121 (10)

All molecules herein reported are asymmetric in their solid-state structures because of the discussed H(hydride) distribution. Therefore attention must be paid when the presence of asymmetric carbon atoms (C* hereafter), as in **2a** and **2b**, implies occurrence of two diastereoisomeric forms. Such diastereomers for **2a** are shown in Scheme II. In both **2a** and **2b** solid-state structures only one of these forms is present for each molecule, though as racemic mixtures of the two enantiomers. It must be pointed out that the existence of form "B" for **2a** (and analogously for a form "B" for *2b*) is due to the different distribution of H atoms with respect to form "A" and is therefore significant only in the solid state. The above mentioned fluxionality of the H atoms, even at low temperature, renders forms "A" and "B" indistinguishable by NMR. On the other hand the presence of conformers of the kind shown in Scheme I may well be possible in solution. Clearly the process of "freezing" the H atoms around the Ru polyhedra in the solid state introduces a further level of asymmetry in the molecule. Compound **2a** has been found to possess a structure in which C* is bonded only to the P atom that is on the side of the Ru atom involved in two H bridges (form "A"). Analogously

Table VI. Fractional Atomic Coordinates and Thermal Parameters ($Å^2$) for **2b**

atom	x	y	z	U_{iso} or U_{eq}
Ru(1)	0.78086 (8)	0.23774 (7)	0.74917 (6)	0.0357 (6)
Ru(2)	0.78653 (10)	0.03410 (8)	0.82833 (7)	0.0464 (6)
Ru(3)	0.57108 (9)	0.05871 (8)	0.72014 (7)	0.0433 (6)
Ru(4)	0.78889 (10)	0.04247 (8)	0.64682 (7)	0.0443 (6)
P(1)	0.7219 (3)	0.3638 (2)	0.8382 (2)	0.039 (2)
P(2)	0.9724 (3)	0.3379 (2)	0.7751 (2)	0.039 (2)
C(1)	0.7545 (12)	0.3084 (10)	0.6530 (9)	0.054 (3)
O(1)	0.7406 (10)	0.3509 (8)	0.5890 (7)	0.077 (3)
C(2)	0.7634 (13)	−0.1033 (12)	0.8064 (10)	0.062 (4)
O(2)	0.7435 (11)	−0.1942 (10)	0.7965 (8)	0.094 (4)
C(3)	0.9544 (15)	0.0431 (12)	0.8271 (11)	0.072 (4)
O(3)	1.0614 (12)	0.0531 (9)	0.8282 (8)	0.097 (4)
C(4)	0.7761 (17)	0.0317 (14)	0.9496 (13)	0.089 (5)
O(4)	0.7679 (16)	0.0292 (13)	1.0242 (13)	0.146 (6)
C(5)	0.5192 (14)	0.0950 (12)	0.6104 (11)	0.071 (4)
O(5)	0.4844 (12)	0.1233 (10)	0.5422 (9)	0.111 (4)
C(6)	0.5059 (14)	−0.0816 (12)	0.6964 (10)	0.069 (4)
O(6)	0.4610 (11)	−0.1674 (9)	0.6826 (8)	0.087 (3)
C(7)	0.4340 (15)	0.0829 (12)	0.7757 (11)	0.075 (4)
O(7)	0.3478 (14)	0.1022 (11)	0.8117 (10)	0.119 (5)
C(8)	0.7283 (12)	−0.0960 (11)	0.6172 (9)	0.055 (3)
O(8)	0.6961 (9)	−0.1811 (8)	0.5943 (7)	0.075 (3)
C(9)	0.9446 (14)	0.0251 (11)	0.6251 (10)	0.066 (4)
O(9)	1.0428 (12)	0.0133 (10)	0.6102 (9)	0.102 (4)
C(10)	0.7572 (14)	0.0787 (12)	0.5358 (11)	0.070 (4)
O(10)	0.7340 (12)	0.1040 (10)	0.4628 (9)	0.105 (4)
C(12)	0.5085 (7)	0.3862 (5)	0.7481 (6)	0.064 (4)
C(13)	0.4344 (7)	0.4359 (5)	0.6954 (6)	0.068 (4)
C(14)	0.4768 (7)	0.5369 (5)	0.6730 (6)	0.071 (4)
C(15)	0.5932 (7)	0.5882 (5)	0.7032 (6)	0.066 (4)
C(16)	0.6673 (7)	0.5386 (5)	0.7558 (6)	0.054 (3)
C(11)	0.6249 (7)	0.4376 (5)	0.7783 (6)	0.044 (3)
C(18)	0.6303 (8)	0.4197 (5)	0.9947 (5)	0.058 (3)
C(19)	0.5811 (8)	0.4004 (5)	1.0758 (5)	0.062 (4)
C(20)	0.5484 (8)	0.2993 (5)	1.1009 (5)	0.074 (4)
C(21)	0.5650 (8)	0.2174 (5)	1.0449 (5)	0.074 (4)
C(22)	0.6142 (8)	0.2367 (5)	0.9638 (5)	0.061 (4)
C(17)	0.6469 (8)	0.3378 (5)	0.9387 (5)	0.045 (3)
C(24)	1.1105 (9)	0.2661 (6)	0.6521 (6)	0.067 (4)
C(25)	1.1715 (9)	0.2681 (6)	0.5746 (6)	0.092 (5)
C(26)	1.1830 (9)	0.3545 (6)	0.5242 (6)	0.101 (6)
C(27)	1.1336 (9)	0.4390 (6)	0.5514 (6)	0.087 (5)
C(28)	1.0726 (9)	0.4370 (6)	0.6288 (6)	0.073 (4)
C(23)	1.0611 (9)	0.3505 (6)	0.6792 (6)	0.057 (3)
C(30)	1.1992 (7)	0.3257 (6)	0.8553 (4)	0.050 (3)
C(31)	1.2762 (7)	0.3076 (6)	0.9255 (4)	0.065 (4)
C(32)	1.2276 (7)	0.2717 (6)	1.0032 (4)	0.069 (4)
C(33)	1.1021 (7)	0.2539 (6)	1.0106 (4)	0.067 (4)
C(34)	1.0251 (7)	0.2720 (6)	0.9404 (4)	0.050 (3)
C(29)	1.0737 (7)	0.3079 (6)	0.8627 (4)	0.043 (3)
C(35)	0.9540 (11)	0.4702 (9)	0.8096 (8)	0.044 (3)
C(36)	0.8566 (11)	0.4565 (9)	0.8788 (8)	0.050 (3)
C(37)	1.0728 (12)	0.5430 (10)	0.8488 (9)	0.057 (3)
C(38)	0.8713 (18)	0.2126 (20)	0.3001 (16)	0.054
Cl(1)	1.0197 (10)	0.2638 (9)	0.3052 (10)	0.116 (10)
Cl(2)	0.8195 (13)	0.1810 (10)	0.1959 (9)	0.115 (11)

Table VII. Fractional Atomic Coordinates and Thermal Parameters ($Å^2$) for **3**

atom	x	y	z	U_{iso} or U_{eq}
Ru(1)	0.21981 (11)	0.11550 (5)	0.15794 (5)	0.0322 (6)
Ru(2)	0.11371 (12)	0.06239 (6)	0.27876 (5)	0.0396 (6)
Ru(3)	−0.01058 (11)	0.01155 (5)	0.16537 (5)	0.0352 (6)
Ru(4)	0.28636 (12)	−0.01409 (6)	0.20492 (5)	0.0438 (7)
P(1)	0.0904 (3)	0.2120 (2)	0.1431 (1)	0.033 (2)
P(2)	−0.0145 (4)	0.1428 (2)	0.3310 (1)	0.043 (2)
C(1)	0.2766 (17)	0.1098 (7)	0.0777 (7)	0.059 (4)
O(1)	0.3101 (14)	0.1043 (6)	0.0276 (6)	0.095 (4)
C(2)	0.3971 (20)	0.1554 (8)	0.1815 (8)	0.073 (5)
O(2)	0.4999 (17)	0.1847 (7)	0.2002 (6)	0.116 (5)
C(3)	0.0319 (18)	−0.0037 (8)	0.3240 (8)	0.072 (5)
O(3)	−0.0283 (15)	−0.0398 (7)	0.3517 (6)	0.102 (4)
C(4)	0.2812 (18)	0.0649 (8)	0.3308 (7)	0.068 (4)
O(4)	0.3787 (13)	0.0623 (6)	0.3661 (5)	0.085 (3)
C(5)	−0.2118 (17)	0.0350 (7)	0.1396 (7)	0.060 (4)
O(5)	−0.3321 (13)	0.0473 (6)	0.1211 (5)	0.085 (4)
C(6)	0.0479 (15)	−0.0257 (7)	0.0924 (6)	0.049 (4)
O(6)	0.0756 (12)	−0.0453 (5)	0.0456 (5)	0.078 (3)
C(7)	−0.0709 (17)	−0.0641 (8)	0.1989 (7)	0.062 (4)
O(7)	−0.1105 (14)	−0.1134 (6)	0.2202 (6)	0.095 (4)
C(8)	0.4763 (17)	0.0007 (7)	0.2427 (7)	0.058 (4)
O(8)	0.5933 (13)	0.0094 (6)	0.2637 (5)	0.083 (3)
C(9)	0.3563 (21)	−0.0641 (9)	0.1437 (9)	0.090 (6)
O(9)	0.4080 (19)	−0.0928 (8)	0.1044 (8)	0.142 (6)
C(10)	0.2437 (22)	−0.0802 (10)	0.2544 (9)	0.097 (6)
O(10)	0.2216 (19)	−0.1270 (8)	0.2853 (8)	0.142 (6)
C(12)	0.2442 (11)	0.2873 (5)	0.0601 (4)	0.066 (4)
C(13)	0.3377 (11)	0.3374 (5)	0.0433 (4)	0.086 (5)
C(14)	0.4013 (11)	0.3771 (5)	0.0873 (4)	0.094 (6)
C(15)	0.3714 (11)	0.3666 (5)	0.1482 (4)	0.123 (8)
C(16)	0.2779 (11)	0.3164 (5)	0.1650 (4)	0.092 (6)
C(11)	0.2143 (11)	0.2768 (5)	0.1209 (4)	0.043 (3)
C(18)	−0.1130 (9)	0.1645 (3)	0.0539 (4)	0.047 (3)
C(19)	−0.2393 (9)	0.1691 (3)	0.0151 (4)	0.059 (4)
C(20)	−0.3167 (9)	0.2264 (3)	0.0091 (4)	0.065 (4)
C(21)	−0.2678 (9)	0.2792 (3)	0.0419 (4)	0.073 (5)
C(22)	−0.1416 (9)	0.2746 (3)	0.0807 (4)	0.057 (4)
C(17)	−0.0641 (9)	0.2173 (3)	0.0867 (4)	0.031 (3)
C(24)	−0.0052 (8)	0.1079 (4)	0.4517 (4)	0.058 (4)
C(25)	−0.0602 (8)	0.0783 (4)	0.5033 (4)	0.062 (4)
C(26)	−0.2085 (8)	0.0548 (4)	0.5037 (4)	0.070 (5)
C(27)	−0.3019 (8)	0.0608 (4)	0.4524 (4)	0.073 (5)
C(28)	−0.2470 (8)	0.0904 (4)	0.4008 (4)	0.063 (4)
C(23)	−0.0986 (8)	0.1139 (4)	0.4005 (4)	0.046 (3)
C(30)	0.0398 (7)	0.2533 (4)	0.3979 (4)	0.053 (4)
C(31)	0.1262 (7)	0.3048 (4)	0.4181 (4)	0.062 (4)
C(32)	0.2769 (7)	0.3114 (4)	0.4002 (4)	0.077 (5)
C(33)	0.3413 (7)	0.2665 (4)	0.3622 (4)	0.065 (4)
C(34)	0.2550 (7)	0.2151 (4)	0.3419 (4)	0.051 (4)
C(29)	0.1043 (7)	0.2085 (4)	0.3598 (4)	0.039 (3)
C(35)	−0.0024 (13)	0.2409 (6)	0.2122 (5)	0.040 (3)
C(36)	−0.1432 (14)	0.1996 (6)	0.2253 (6)	0.045 (3)
C(37)	−0.1718 (14)	0.1858 (6)	0.2909 (6)	0.047 (3)

2b possesses only the form in which the P atom linked to C* is radially bonded to Ru(1). These choices (with respect to several other possibilities) depend upon subtle energy differences.

Experimental Section

All reactions were carried out under purified nitrogen. Solvents were distilled under nitrogen and dried prior to use. Infrared spectra were recorded on a Perkin-Elmer 1320 spectrophotometer. The ^1H NMR spectra were measured with use of a Varian XL-100 spectrometer. The ^{31}P NMR spectra were recorded at 24.289 MHz on a Bruker WP-60 spectrometer. ^1H and ^{31}P chemical shifts are given relative to Me_4Si and H_3PO_4 respectively.

Preparation of $(\mu\text{-H})_4Ru_4(CO)_{10}(\mu\text{-}\{Ph_2P(CH_2)_nPPh_2\})$ (n = 1 (1), 3 (3), 4 (4)) and $(\mu\text{-H})_4Ru_4(CO)_{10}(\mu\text{-}\{Ph_2PCH_2CH(CH_3)PPh_2\})$ (2a). In a typical experiment trimethylamine N-oxide (20 mg, 0.27 mmol) dissolved in acetonitrile (45 mL) was added dropwise to a solution of $(\mu\text{-H})_4Ru_4(CO)_{12}$ (300 mg, 0.40 mmol) and $Ph_2PCH_2PPh_2$ (190 mg, 0.49 mmol) in CH_2Cl_2 (250 mL). The originally yellow reaction mixture became red in color. The solution was stirred for ca. 1 h at room temperature and filtered through a short silica column, and the volume was reduced under vacuum. Thin-layer chromatography using a 3:1 hexane–toluene mixture as eluent gave a red band, which was extracted with CH_2Cl_2. Dark red crystals were obtained upon crystallization from a CH_2Cl_2–CH_3OH mixture [yields (based on the amount of Me_3NO used): **1** = 83 mg, 58%, **2a** = 97 mg, 66%; **3** = 36 mg, 25%; **4** = 44 mg, 30%]. Compounds **1**, **2a**, **3**, and **4** were characterized by IR, ^1H NMR, and ^{31}P NMR spectroscopy (Table I).

Preparation of $[(\mu\text{-H})_4Ru_4(CO)_{11}]_2\{Ph_2P(CH_2)_5PPh_2\}$ (5a) and 5b. Trimethylamine N-oxide (15 mg, 0.2 mmol) dissolved in acetonitrile (45 mL) was added dropwise to a solution of $(\mu\text{-H})_4Ru_4(CO)_{12}$ (300 mg, 0.40 mmol) and $Ph_2P(CH_2)_5PPh_2$ (215 mg, 0.49 mmol) in CH_2Cl_2 (350 mL). The solution was stirred for ca. 1 h and filtered through a short silica column. Thin-layer chromatography using a 3:5 toluene–hexane mixture gave a red band and orange bands, which are difficult to separate. These two bands were extracted with CH_2Cl_2 and tlc by using hexane as eluent. The red (**5a**) and orange (**5b**) compounds were crystallized from a CH_2Cl_2–CH_3OH mixture (yields: **5a** = 32 mg, 17%; **5b** = 64 mg) and characterized by IR, ^1H NMR, and ^{31}P NMR spectroscopy (Table I).

Preparation of $(\mu\text{-H}_4)Ru_4(CO)_{10}\{Ph_2PCH_2CH(CH_3)PPh_2\}$ (2b). $(\mu\text{-H})_4Ru_4(CO)_{12}$ (150 mg, 0.20 mmol) and $Ph_2PCH_2CH(CH_3)PPh_2$ (96.3 mg, 0.23 mmol) were refluxed in cyclohexane for 8 h. The reaction was

Table VIII. Fractional Atomic Coordinates and Thermal Parameters ($Å^2$) for **4**

atom	x	y	z	U_{iso} or U_{eq}
Ru(1)	0.32812	0.09618 (4)	−0.05101	0.0380 (6)
Ru(2)	0.51991 (17)	0.07074 (5)	0.07268 (7)	0.0448 (7)
Ru(3)	0.59383 (17)	0.01211 (5)	−0.03865 (8)	0.0446 (7)
Ru(4)	0.34530 (18)	−0.02515 (5)	0.01327 (8)	0.0492 (7)
P(1)	0.3945 (4)	0.1904 (1)	−0.0896 (2)	0.036 (2)
P(2)	0.6746 (4)	0.1533 (2)	0.1172 (2)	0.039 (2)
C(1)	0.2183 (17)	0.0736 (7)	−0.1286 (8)	0.059 (4)
O(1)	0.1528 (14)	0.0601 (6)	−0.1746 (6)	0.086 (4)
C(2)	0.1608 (18)	0.1306 (7)	−0.0256 (7)	0.058 (4)
O(2)	0.0588 (16)	0.1529 (6)	−0.0083 (6)	0.097 (4)
C(3)	0.6161 (18)	0.0147 (8)	0.1262 (8)	0.066 (4)
O(3)	0.6883 (15)	−0.0193 (6)	0.1618 (7)	0.099 (4)
C(4)	0.3808 (20)	0.0822 (8)	0.1199 (9)	0.072 (5)
O(4)	0.2934 (18)	0.0933 (6)	0.1548 (7)	0.112 (5)
C(5)	0.7035 (19)	−0.0529 (8)	−0.0009 (8)	0.067 (4)
O(5)	0.7816 (15)	−0.0950 (6)	0.0197 (6)	0.094 (4)
C(6)	0.7600 (20)	0.0420 (8)	−0.0710 (8)	0.066 (4)
O(6)	0.8624 (17)	0.0592 (7)	−0.0945 (7)	0.105 (4)
C(7)	0.4967 (19)	−0.0309 (7)	−0.1072 (8)	0.066 (4)
O(7)	0.4326 (14)	−0.0542 (6)	−0.1525 (6)	0.087 (4)
C(8)	0.2428 (19)	−0.0804 (8)	−0.0440 (8)	0.064 (5)
O(8)	0.1808 (14)	−0.1193 (6)	−0.0765 (6)	0.089 (4)
C(9)	0.1937 (23)	−0.0215 (10)	0.0604 (11)	0.093 (6)
O(9)	0.0998 (20)	−0.0193 (8)	0.0902 (8)	0.136 (6)
C(10)	0.4515 (20)	−0.0866 (8)	0.0606 (9)	0.070 (5)
O(10)	0.5084 (16)	−0.1275 (6)	0.0892 (7)	0.102 (4)
C(12)	0.1801 (9)	0.2787 (4)	−0.0681 (3)	0.050 (4)
C(13)	0.0386 (9)	0.3079 (4)	−0.0814 (3)	0.066 (4)
C(14)	−0.0586 (9)	0.2966 (4)	−0.1372 (3)	0.066 (4)
C(15)	−0.0144 (9)	0.2560 (4)	−0.1796 (3)	0.067 (4)
C(16)	0.1272 (9)	0.2268 (4)	−0.1663 (3)	0.056 (4)
C(11)	0.2244 (9)	0.2382 (4)	−0.1106 (3)	0.044 (3)
C(18)	0.5069 (11)	0.2476 (3)	−0.1823 (4)	0.050 (4)
C(19)	0.5689 (11)	0.2513 (3)	−0.2357 (4)	0.069 (5)
C(20)	0.5992 (11)	0.1976 (3)	−0.2660 (4)	0.075 (5)
C(21)	0.5675 (11)	0.1402 (3)	−0.2429 (4)	0.081 (5)
C(22)	0.5055 (11)	0.1365 (3)	−0.1895 (4)	0.065 (4)
C(17)	0.4751 (11)	0.1902 (3)	−0.1592 (4)	0.040 (3)
C(24)	0.7048 (9)	0.1306 (4)	0.2423 (5)	0.054 (4)
C(25)	0.7752 (9)	0.1053 (4)	0.2982 (5)	0.068 (4)
C(26)	0.9165 (9)	0.0763 (4)	0.3030 (5)	0.078 (5)
C(27)	0.9875 (9)	0.0727 (4)	0.2519 (5)	0.076 (5)
C(28)	0.9171 (9)	0.0981 (4)	0.1960 (5)	0.062 (4)
C(23)	0.7758 (9)	0.1270 (4)	0.1912 (5)	0.049 (3)
C(30)	0.4288 (9)	0.2342 (4)	0.1129 (4)	0.050 (4)
C(31)	0.3615 (9)	0.2908 (4)	0.1216 (4)	0.072 (5)
C(32)	0.4491 (9)	0.3381 (4)	0.1528 (4)	0.080 (5)
C(33)	0.6040 (9)	0.3289 (4)	0.1754 (4)	0.075 (5)
C(34)	0.6713 (9)	0.2723 (4)	0.1667 (4)	0.057 (4)
C(29)	0.5837 (9)	0.2250 (4)	0.1355 (4)	0.047 (3)
C(35)	0.8321 (15)	0.1835 (6)	0.0820 (7)	0.046 (3)
C(36)	0.7910 (17)	0.2322 (7)	0.0315 (7)	0.055 (4)
C(37)	0.6889 (15)	0.2082 (7)	−0.0272 (7)	0.052 (4)
C(38)	0.5291 (14)	0.2363 (6)	−0.0386 (7)	0.043 (3)

monitored by IR spectroscopy. The solvent was evaporated to dryness under vacuum and the residue dissolved in $CHCl_3$ (5 mL). Thin-layer chromatography using a 5:1 toluene–hexane mixture as eluent gave a red band, which was extracted with CH_2Cl_2. Dark red crystals were obtained from a CH_2Cl_2–CH_3OH mixture (yield 80 mg, 36%). Compound **2b** was characterized by IR, ^1H NMR, and ^{31}P NMR spectroscopy (Table I). The title complex can also be prepared by refluxing the *bridged* derivative $(\mu\text{-H})_4Ru_4(CO)_{10}(\mu\text{-}\{Ph_2PCH_2CH(CH_3)PPh_2\})$ (30 mg, 0.027 mmol) in $CDCl_3$ (3 mL) for ca. 1.5 h. The reaction was monitored by ^{31}P NMR spectroscopy. Dark red crystals were obtained from a CH_2Cl_2–CH_3OH mixture (yield 20 mg, 65%).

Thermolysis of $(\mu\text{-H})_4Ru_4(CO)_{10}(\mu\text{-}\{Ph_2PCH_2PPh_2\})$ (1). $(\mu\text{-H})_4Ru_4(CO)_{10}\{\mu\text{-}Ph_2PCH_2PPh_2\}$ (25 mg, 0.023 mmol) was refluxed in cyclohexane (50 mL) for 10 h. The reaction was monitored by IR spectroscopy. Decomposition was observed over this period of time. Formation of the chelate isomer was not detected.

X-ray Structural Determination. Crystal data and details of measurements for **1**, **2a**, **2b**, **3**, and **4** are contained in Table III. Diffraction intensities for all crystals were collected at room temperature on an Enraf-Nonius CAD-4 diffractometer equipped with Mo Kα radiation (λ = 0.71069 Å) reduced to F_o values and corrected for crystal decay when necessary. An empirical absorption correction was applied either by measuring azimuthal reflections (X > 80°) of suitable intensities or by employing the Walker and Stuart method[12] once the structural models were completely defined and all atoms refined isotropically. The metal atom positions were determined either by conventional Patterson or by direct methods; in the latter case the MITHRIL package was used.[13] All light atoms were located by subsequent Fourier difference maps. Refinement of the models were carried out by full-matrix least-squares calculations. For all computations the SHELX[14] package of crystallographic programs was used, with the analytical scattering factors, corrected for real and imaginary parts of anomalous dispersion, taken from ref 15. Thermal vibrations were treated anisotropically for Ru and P atoms. Phenyl groups of the phosphine ligands were treated as rigid bodies (C–C 1.395 Å; C–C–C 120°); H atoms were added in calculated positions (C–H 1.08 A) and not refined, though their contribution to the structure factors was taken into account. Attempts to directly locate the H(hydride) atom positions from Fourier difference maps gave contradictory results even when a reduced reflection sphere [$(\sin\theta)/\lambda < 0.30$] was used and were not trusted. In the case of compound **2b**, a partially disordered image of a CH_2Cl_2 solvent molecule was detected in the relative Fourier maps; its occupancy refined to 0.45. For all compounds residual peaks in the final maps never exceeded 1 e/Å^3 and were mainly located in the vicinity of the Ru atoms. Final atomic coordinates for **1**, **2a**, **2b**, **3**, and **4** are listed in Tables IV–VIII, respectively.

Acknowledgment. We gratefully acknowledge CONICIT (Venezuela) for financial support. We are also grateful to Prof. V. G. Albano for a helpful discussion and to Dr. R. A. Sánchez-Delgado for reading the manuscript.

Supplementary Material Available: Tables of anisotropic thermal parameters, fractional atomic coordinates for the hydrogen atoms, and bonds, contacts, and angles for **1**, **2a**, **2b**, **3**, and **4** (78 pages); F_o/F_c tables (77 pages). Ordering information is given on any current masthead page.

(12) Walker, N.; Stuart, D. *Acta Crystallogr., Sect A: Found. Crystallogr.* **1983**, *A39*, 158.
(13) Gilmore, C. J. "MITHRIL, Direct Methods Program", The University of Glasgow, Glasgow, Great Britain, *1980*.
(14) Sheldrick, G. M. "SHELX76, Program for Crystal Structure Determination", University of Cambridge, Cambridge, Great Britain, 1976.
(15) *International Tables for X-ray Crystallography*; Kynoch: Birmingham, Great Britain, 1975; Vol. IV, pp 99–149.